NANO · MICRO small
www.small-journal.com

A Versatile Electrochemical Biosensor for the Detection of Circulating MicroRNA toward Non-Small Cell Lung Cancer Diagnosis

Fanyu Meng, Wenjun Yu, Changqiang Chen, Susu Guo, Xiaoting Tian, Yayou Miao, Lifang Ma, Xiao Zhang, Yongchun Yu, Lin Huang, Kun Qian, and Jiayi Wang**

Circulating microRNAs (miRNAs) can be used as noninvasive biomarkers and are also found circulating in body fluids such as blood. Dysregulated miRNA expression is associated with many diseases, including non-small cell lung cancer (NSCLC), and the miRNA assay is helpful in cancer diagnosis, prognosis, and monitoring. In this work, a versatile electrochemical biosensing system is developed for miRNA detection by DNAzyme-cleavage cycling amplification and hybridization chain reaction (HCR) amplification. With cleavage by Mn^{2+} targeted DNAzyme, DNA-walker can move along the predesigned DNA tracks and contribute to the transduction and enhancement of signals. For the electrochemical process, the formation of multiple G-quadruplex-incorporated long double-stranded DNA (dsDNA/G-quadruplex) structures is triggered through HCR amplification. The introduction of G-quadruplex allows sensitive measurement of miRNA down to 5.68 fM with good specificity. Furthermore, by profiling miRNA in the NSCLC cohort, this designed strategy shows high efficiency (area under the curve (AUC) of 0.879 using receiver operating characteristic (ROC) analysis) with the sensitivity of 80.0% for NSCLC early diagnosis (stage I). For the discrimination of NSCLC and benign disease, the assay displays an AUC of 0.907, superior to six clinically-acceptable protein tumor markers. Therefore, this platform holds promise in clinical application toward NSCLC diagnosis and prognosis.

1. Introduction

Lung cancer (LC) is one of the most common malignancies and the leading cause of about a quarter of cancer-related deaths worldwide (2.09 million new cases and 1.76 million deaths in 2018).[1] Early detection is the key to reducing LC mortality, with overall five-year survival varying 65%–85%, but below 18% in the case of advanced LC patients.[2] Among all LC, non-small cell lung cancer (NSCLC) accounts for approximately 85%.[3] Standard diagnostic procedures such as tumor tissue biopsies are highly invasive and thus are limited in early disease detection.[4] Clinically, regular low-dose computerized tomography is recommended for LC screening while inevitably causing radiation exposure and displaying a high false-positive rate of up to 26%.[5] Therefore, it is pressing to develop a rapid and non-invasive method to discover biomarkers and diagnose early LC with an improved prognosis.[6]

Liquid biopsy allows the tracking of molecular markers through noninvasive techniques from body fluids (typically blood), holding promise for early screening of NSCLC in clinical scenarios.[7] Protein biomarkers (e.g., neuron-specific enolase (NSE) and cytokeratin 19 fragment (CYFRA21-1) have been clinically approved for the vital monitoring of adjuvant therapy in LC, of which value in early screening are concerned due to the lack of sensitivity.[8] Besides proteins, microRNAs (miRNA) regulate gene

F. Meng, W. Yu, L. Ma, X. Zhang, L. Huang, J. Wang
Country Department of Clinical Laboratory Medicine
Shanghai Chest Hospital
Shanghai Jiao Tong University
Shanghai 200030, China
E-mail: jiayi.wang@sjtu.edu.cn

F. Meng, S. Guo, X. Tian, Y. Miao, L. Ma, X. Zhang, Y. Yu, L. Huang, J. Wang
Shanghai Institute of Thoracic Oncology
Shanghai Chest Hospital
Shanghai Jiao Tong University
Shanghai 200030, China

The ORCID identification number(s) for the author(s) of this article can be found under https://doi.org/10.1002/smll.202200784.

C. Chen
Department of Laboratory Medicine
Ruijin Hospital
Shanghai Jiao Tong University School of Medicine
Shanghai 201801, China

K. Qian
State Key Laboratory for Oncogenes and Related Genes
School of Biomedical Engineering
Institute of Medical Robotics and Med-X Research Institute
Shanghai Jiao Tong University
Shanghai 200030, China
E-mail: k.qian@sjtu.edu.cn

DOI: 10.1002/smll.202200784

© 2022 Wiley-VCH GmbH

Check for updates
16136829, 2022, 22, Downloaded from https://onlinelibrary.wiley.com/doi/10.1002/smll.202200784 by Egyptian National Sci. Network (Enstine), Wiley Online Library on [06/11/2022]. See the Terms and Conditions (https://onlinelibrary.wiley.com/terms-and-conditions) on Wiley Online Library for rules of use; OA articles are governed by the applicable Creative Commons License

expression or cellular processes, the dysregulated expression of which is closely related to lung carcinogenesis.[9] Traditional miRNA detection relies on northern blotting, real-time (RT)-PCR, microarrays, and next-generation sequencing, while these methods suffer from intrinsic drawbacks, such as the expensive instruments, complex operations, long analysis time, and professional skills.[10]

The electrochemical biosensor is a powerful analytical tool capable of low-cost, sensitive, and rapid detection of miRNA markers.[11] In particular, signal amplification techniques play vital roles in enhancing sensing sensitivity,[12] including nucleic acid amplification (e.g., DNA walker and hybridization chain reaction (HCR)) and electrical signal molecule amplification (e.g., labeled dyes, nanomaterials, and organic molecules).[13] For DNA walkers, the electrochemical biosensor usually utilizes complex nanocomposites for walker DNA combination, requires a special electrochemical indicator as its signal, or needs the strict reaction conditions for tool enzymes.[14] For HCR, the amplification reaction on the electrode includes tedious modification processes resulting in the clustering of probes and interface identification, which can significantly suppress analytical properties.[15] For electrical signal molecules, the high-cost labeling of oligonucleotides or the uneasy synthesis of nanomaterials may limit their large-scale application in lateral clinical practice.[16] In this way, DNAzyme functionalized AuNPs (as a DNA walker) were applied for target conversion and amplification, and the output molecules were directly used for the electrochemical system, avoiding the complex fabrication process.[17] In addition, G-quadruplex/dsDNA structures could be introduced to the electrochemical system through HCR reaction for the second signal amplification. The methylene blue (MB) could be used as a signal molecule without costly oligonucleotides labeling, and the binding of MB with G-quadruplex structures through π–π stacking interactions is superior to double-stranded DNA.[18] Currently, few works validated the proposed sensor in clinical samples, especially for the diagnosis and prognosis of NSCLC. Therefore, a versatile electrochemical biosensor with dual signal amplification and label-free G-quadruplex/dsDNA structures would fit in the simplified clinical workflow in NSCLC management.

In this work, we developed an integrated electrochemical platform based on DNAzyme-cleavage cycling amplification and HCR amplification for miRNA detection. We introduced the G-quadruplex/dsDNA structure for signal amplification on the electrode surface and evaluated the detection performance of this method. The designed biosensor showed a detection limit of 5.68 fM within a wide linear range from 20 fM to 5 nM. We validated the biosensing system through both the NSCLC-related cell lines and a retrospective cohort. As a result, the facile miRNA detection based on the sensor yielded high sensitivity of 80.0% and specificity of 78.6% for the discrimination of early NSCLC patients from healthy controls. For the discrimination of NSCLC and benign disease, the assay was superior to the analysis of other six clinically-acceptable protein tumor markers, with an area under the curve (AUC) of 0.907 using receiver operating characteristic (ROC) analysis (sensitivity of 86.7% and specificity of 73.3%). Our work opens new possibilities to improve the surveillance of NSCLC, using fast and minimally invasive blood analysis towards precision diagnosis in clinical situations.

2. Results and Discussion

2.1. Principle of the Electrochemical MiRNA Assay

The principle of the electrochemical strategy based on DNAzyme-cleavage cycling amplification and HCR amplification for miRNA detection is illustrated in **Scheme 1**. First, the target miRNA displaces the DNAzyme strand to completely hybridize with the locking strand, enabling release into solution from the functionalized AuNPs. Then, MnO_2 nanosheets are reduced to manganese ion (Mn^{2+}) by glutathione (GSH), and Mn^{2+} participates in a DNAzyme cleavage-cycling reaction to produce a large number of output DNA molecules. Next, the output DNA is introduced to the electrochemical process. Two species of metastable hairpin DNA (H1 and H2) are designed, in which H1 contained sequences partially complementary to the output DNA, as well as to H2. In the presence of output DNA, H1 is unfolded via hybridization with the output DNA to trigger the autonomous cross-opening of the two hairpin DNAs through the toehold-mediated strand displacement reaction, generating a long chain of double-stranded DNA (dsDNA). With the aid of K^+ ions, multiple G-quadruplexes are incorporated at both ends of H1 and H2, resulting in the formation of multiple G-quadruplex-incorporated long duplex DNA chains (dsDNA/G-quadruplexes). With MB selectively intercalated into the dsDNA/G-quadruplex structure, the electrochemical signal is greatly enhanced, proportional to the concentration of the target miRNA. Thus, a label-free electrochemical strategy based on DNAzyme and HCR amplification for a sensitive circulating miRNA assay is readily realized. The designed biosensor shows great potential in biological applications for miR-486-5p-related NSCLC monitoring and clinical diagnostics.

2.2. Characterization and Optimization of the Experimental Condition

Transmission electron microscope (TEM) images and ultraviolet–visible (UV–vis) absorption spectra were used to characterize the prepared AuNPs and MnO_2 nanosheets. The TEM image showed that the AuNPs were well distributed and had an average diameter of 13 ± 3 nm (**Figure 1**A). TEM image of single entities of AuNPs was consistent with the results (Figure S1A, Supporting Information). In the UV–vis absorption spectrum, the absorption peak of the AuNPs occurred at 520 nm, which was consistent with a previous report (Figure 1C).[19] The dynamic light scattering analysis was performed to explicate the hydrodynamic size of AuNPs (Figure S1B, Supporting Information). As shown in Figure 1B, the TEM image of the MnO_2 nanosheets showed a large 2D and ultrathin surface with folds and wrinkles. In the UV–vis absorption spectrum of the MnO_2 nanosheets, a wide absorption band with a peak at 326 nm was observed (Figure 1C). Mn^{2+} was successfully produced through the reduction of MnO_2 nanosheets by GSH (Figure S1C,D, Supporting Information). To improve the DNAzyme-cleavage

© 2022 Wiley-VCH GmbH

16136829, 2022, 22, Downloaded from https://onlinelibrary.wiley.com/doi/10.1002/smll.202200784 by Egyptian National Sci. Network (Enstine), Wiley Online Library on [06/11/2022]. See the Terms and Conditions (https://onlinelibrary.wiley.com/terms-and-conditions) on Wiley Online Library for rules of use; OA articles are governed by the applicable Creative Commons License

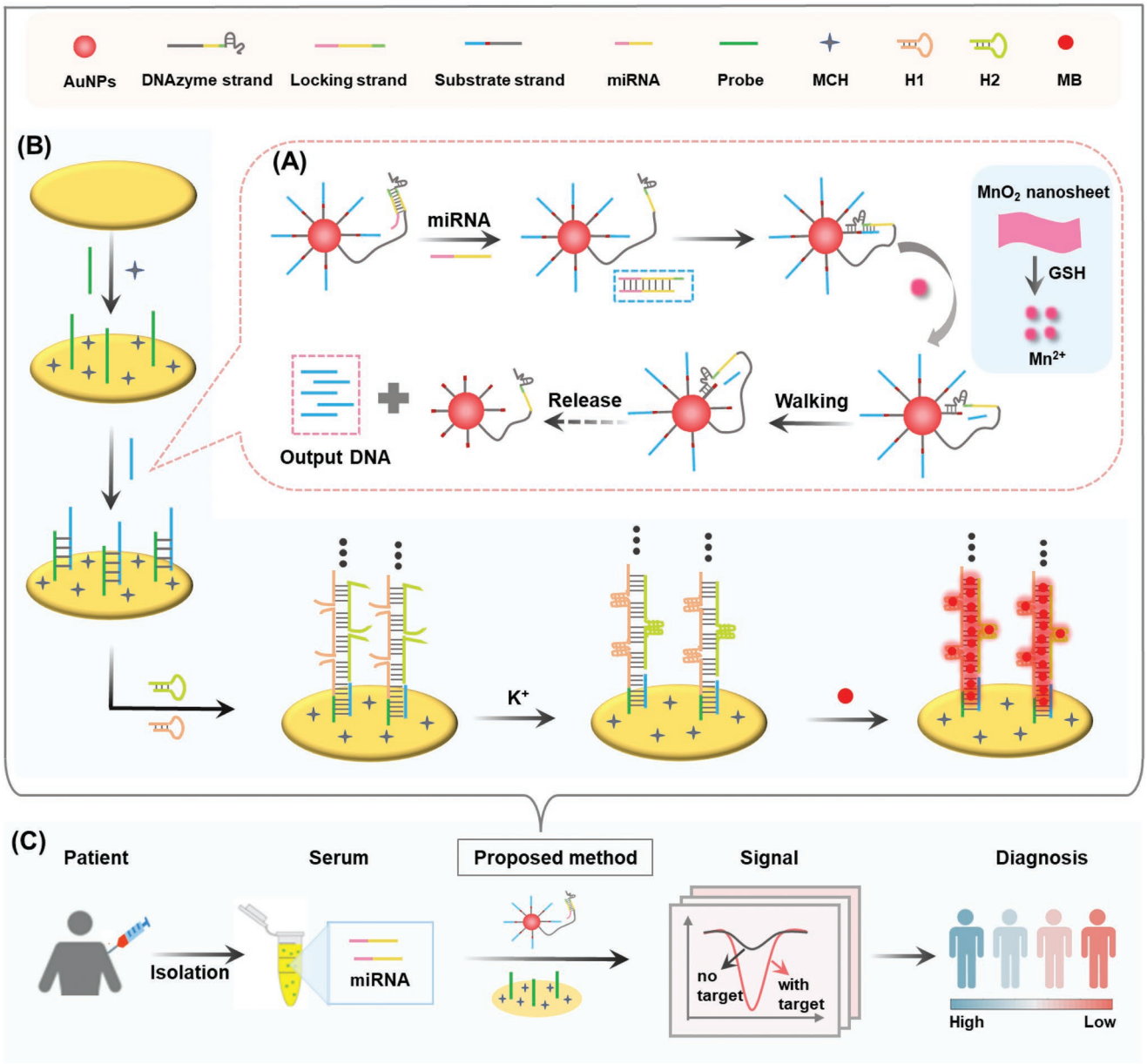

Scheme 1. Principle of the electrochemical strategy for miRNA assay. A) DNAzyme-cleavage cycling amplification. B) hybridization chain reaction (HCR) amplification. C) Workflow for detection of miRNA from patient serum.

cycling amplification efficiency, the concentration of the MnO_2 nanosheets (20 μM) and the operation time of the DNA walker (1.5 h) were investigated (Figure S2A,B, Supporting Information). To improve the HCR amplification efficiency, the MB concentration (50 μM) and the reaction time (2 h) were optimized (Figure S2C,D, Supporting Information).

The effect of the different concentration ratios of DNAzyme to substrate strands is very important because the concentration directly influences the DNAzyme-cleavage cycling amplification reaction.[20] As shown in Figure 1D, different ratios of the DNAzyme and substrate strands were investigated using target miRNA concentrations of 0.5 and 2 pM. Figure 1E shows that there were consistent results for the different concentration ratios of DNAzyme to the substrate, and the linear sweep voltammetry (LSV) intensity reached the highest point of the reaction at 1:20, suggesting that a ratio of 1:20 was sufficient for DNA walking. Thus, the optimum ratio of DNAzyme to substrate was determined to be 1:20 in the procedure.

In order to get a more powerful platform, the DNA conformations of the dsDNA/G-quadruplex structure were studied further. As exhibited in Figure 1F, the dsDNA was formed by P1 and P2 via the target-triggered HCR, and the dsDNA/G-quadruplex structure was likely formed by H1 and H2. The introduction of G-quadruplex would increase the MB signal to the electrode surface, used for cascading amplification. As shown in Figure 1G, dsDNA and dsDNA/G-quadruplex assembled systems were incubated with various concentrations of miR-486-5p, respectively. Relatively stable curves

© 2022 Wiley-VCH GmbH

16136829, 2022, 22, Downloaded from https://onlinelibrary.wiley.com/doi/10.1002/smll.202200784 by Egyptian National Sci. Network (Enstine), Wiley Online Library on [06/11/2022]. See the Terms and Conditions (https://onlinelibrary.wiley.com/terms-and-conditions) on Wiley Online Library for rules of use; OA articles are governed by the applicable Creative Commons License

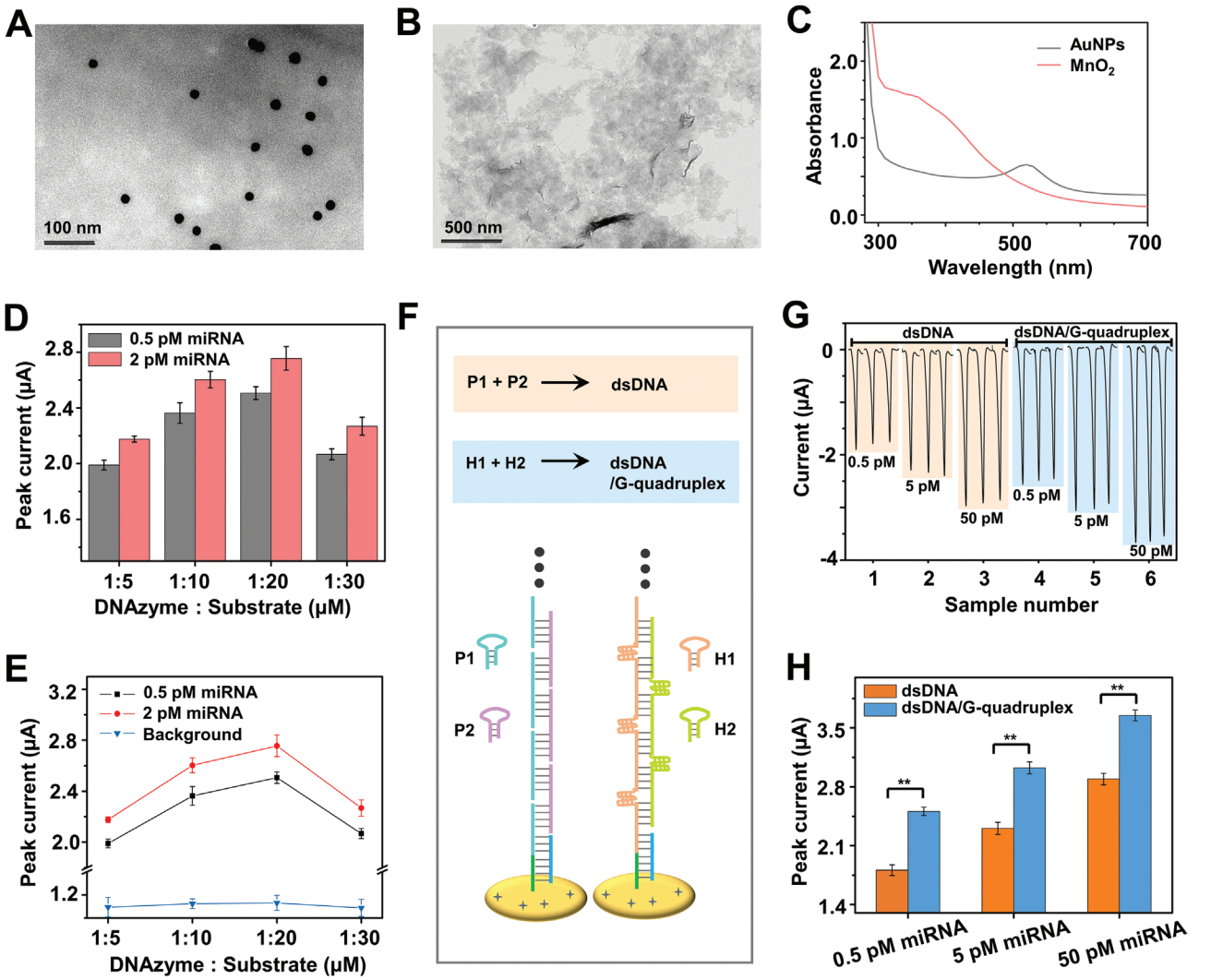

Figure 1. A) Transmission electron microscope (TEM) image of the AuNPs. B) TEM image of the MnO_2 nanosheets. C) UV–vis absorption of the MnO_2 nanosheets and AuNPs. D) The intensity of the electrochemical response on the ratio of DNAzyme to substrate strand. E) The corresponding line chart for different miRNA reactions. F) Schematic illustration of different DNA conformations. G) Linear sweep voltammetry (LSV) and H) the peak current of the hybridization chain reaction (HCR) product for the various concentration of miR-486-5p with dsDNA compared with the dsDNA/G-quadruplex. Statistical significance was tested using a two-tailed Students *t*-test, $^{**}p < 0.01$. LSV detection under different conditions: MB inserted into the dsDNA formed by P1 and P2; MB inserted into the dsDNA/G-quadruplex formed by H1 and H2. The concentrations of P1, P2, H1, H2, and MB were 2 μM, 2 μM, 2 μM, 2 μM, and 50 μM, respectively. The concentrations of miR-486-5p were 0.5 pM, 5 pM, 50 pM, respectively.

were obtained on each concentration by three independent experiments, and the peak current only showed a slight elevation change affording coefficient of variation (CV) within 3.5%, indicating the excellent stability of the biosensor. The reproducibility and stability were also further investigated, as shown in Figure S3 (Supporting Information). The CV was calculated to be 2.6% for different modified electrodes, which indicated the high reproducibility of the proposed method. The electrochemical signals were retained at 91.0% after storage for one week, which indicated the high stability of the proposed method. We confirmed the cycling number of DNAzyme-cleavage amplification reaction was consistent for different tests, based on the experimental procedure and the quantitation results. For the experimental procedure, we employed abundant DNA strands bonded to the surface of AuNPs until saturation. Therefore, the same concentration of miRNA guaranteed the same cycling number of DNAzyme-cleavage amplification reaction, according to previous literature.[21] For the quantitation results, the platform afforded a CV within 3.5%, validating the consistent cycling number of DNAzyme-cleavage amplification reaction for different tests. Then, the binding ability of MB toward different DNA conformations was tested (Figure 1H). When MB was added and inserted into the dsDNA, the peak current of MB was observed to increase with the concentrations of miR-486-5p. However, an even more significant signal ($p < 0.01$) was detected in the presence of MB, H1, and H2, because of the fact that dsDNA/G-quadruplex structure was formed and the intercalation of MB into G-quadruplex further increased the current of MB to the electrode surface. The average enhancement ratio

© 2022 Wiley-VCH GmbH

16136829, 2022, 22, Downloaded from https://onlinelibrary.wiley.com/doi/10.1002/smll.202200784 by Egyptian National Sci. Network (Enstine), Wiley Online Library on [06/11/2022]. See the Terms and Conditions (https://onlinelibrary.wiley.com/terms-and-conditions) on Wiley Online Library for rules of use; OA articles are governed by the applicable Creative Commons License

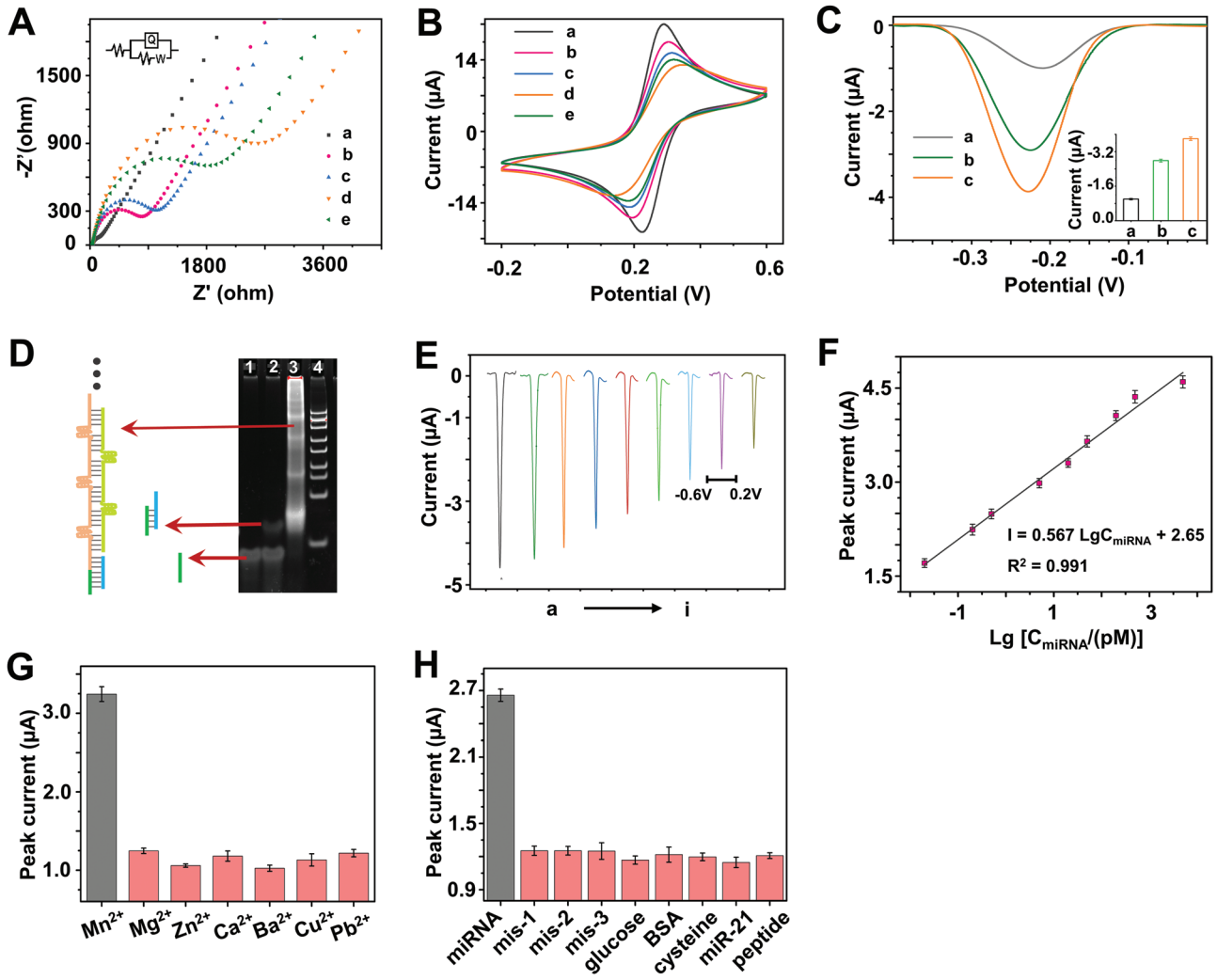

Figure 2. EIS (A) and CV (B) curves of the bare electrode (curve a), bare/probe DNA (curve b), bare/probe DNA/output DNA (curve c), bare/probe DNA/output DNA/H1/H2 (curve d), and bare/probe DNA/output DNA/H1/H2/MB (curve e). C) Linear sweep voltammetry (LSV) of MB signals under different conditions: H1 + H2 (curve a); dsDNA formed by H1 and H2 (curve b); and dsDNA/G-quadruplex formed by H1 and H2 in the presence of K^+ ions (curve c), the inset shows the peak current; the concentrations of MB, H1, H2, and miR-486-5p were 50 μM, 2 μM, 2 μM, and 100 pM, respectively. D) Polyacrylamide gel electrophoresis (PAGE) analysis of probe DNA (lane 1), probe DNA + output DNA (lane 2), and probe DNA + output DNA+H1+H2 (lane 3). E) LSV results for the analysis of miRNA at different concentrations: 5 nM, 500 pM, 200 pM, 50 pM, 20 pM, 5 pM, 500 fM, 200 fM, and 20 fM (from a to i). F) The linear relationship between the absolute value of the LSV peak current and the logarithm of the miR-486-5p concentration. The error bars represent the standard deviation of three independent measurements. G) Selectivity of the biosensor for Mn^{2+} compared with other potential interfering ions: Mg^{2+}; Zn^{2+}; Ca^{2+}; Ba^{2+}; Cu^{2+}; and Pb^{2+} (metal ions: 2 mM, miRNA: 20 pM). H) Selectivity of the biosensor for miRNA detection compared with other potential contaminants: mis-1; mis-2; mis-3; glucose; BSA; cysteine; miR-21; and peptide (miRNA: 1 pM, other compounds: 2 μM).

of the signal was about 32.0%. The results were in accordance with the LSV results shown in **Figure 2**C. Therefore, the introduction of G-quadruplex to the reaction system can help to induce larger changes in electrochemical signal, which would highly improve the sensitivity of the method.

Most electrochemical methods for miRNA detection utilize DNAzyme-cleavage cycling amplification and HCR amplification. However, we designed the amplification reaction with DNAzyme functionalized AuNPs and G-quadruplex/dsDNA structures, avoiding complex nanocomposites, tedious modification processes, and strict enzymes reaction conditions. Particularly, MB was used as a signal molecule without costly oligonucleotides labeling (≈50% savings of total cost), and the detected signal from G-quadruplex/dsDNA structures was superior to dsDNA ($p < 0.01$, ≈30% of signal enhancement ratio).[22] GSH is the most prevalent nonprotein thiol species in biological systems and has an abnormal level in cancer cells.[23] In this platform, MnO_2 was introduced to produce Mn^{2+} in the presence of GSH instead of directly adding Mn^{2+} ions, shedding light on its potential application in GSH quantitation (Figure S2A, Supporting Information). The GSH quantitation is very important for the early diagnosis and therapy of some related diseases, especially cancers. Therefore, the strategy designed herein is cost-effective and easy to implement.

© 2022 Wiley-VCH GmbH

16136829, 2022, 22, Downloaded from https://onlinelibrary.wiley.com/doi/10.1002/smll.202200784 by Egyptian National Sci. Network (Enstine), Wiley Online Library on [06/11/2022]. See the Terms and Conditions (https://onlinelibrary.wiley.com/terms-and-conditions) on Wiley Online Library for rules of use; OA articles are governed by the applicable Creative Commons License

2.3. Fabrication of the Biosensor for MiRNA Detection

Electrochemical impedance spectroscopy (EIS) and cyclic voltammetry (CV) were used to investigate the fabrication process of the biosensor. As shown in Figure 2A, the electron transfer resistance (R_{et}) of $[Fe(CN)_6]^{4-/3-}$ indicated the interfacial changes of the different modified electrodes. Compared with the bare electrode (curve a), an increased semicircle diameter was observed for the successfully modified probe DNA electrode (curve b). Because of the repulsion of $[Fe(CN)_6]^{4-/3-}$by the DNA backbone and mercaptoethanol (MCH), a larger R_{et} value was obtained after introducing output DNA (curve c). A greatly increased impedance value was observed after the addition of H1 and H2 (curve d), suggesting that the output DNA initiated the HCR amplification response on the electrode. After modification with MB, the R_{et} value decreased because MB accelerated the transfer of electrons (curve e). These results indicated the successful fabrication of the biosensor. The electrochemical performance of the biosensor during the fabrication process was also investigated using CV measurements of the current changes. As seen in Figure 2B, the voltammograms of $[Fe(CN)_6]^{4-/3-}$ gradually changed during the modification of the electrodes, which further indicated that the biosensor had been successfully fabricated.

The feasibility of the proposed electrochemical miRNA assay was also investigated. As shown in Figure 2C, in the presence of MB, H1, and H2, a small signal was observed (curve a), indicating that the majority of the MB was not immobilized on the electrode. Once the target miRNA (miR-486-5p) was present in the reaction system and K^+ ions were absent, the results showed an obviously larger signal (curve b), indicating the intercalation of MB into the dsDNA chain formed via the target-triggered HCR. If K^+ ions were present, the electrochemical signal showed a further enhancement (curve c), clearly demonstrating the occurrence of the HCR and the subsequent formation of multiple dsDNA/G-quadruplexes intercalated with MB, which resulted in the current being significantly increased because of the excellent conductivity and electron transfer ability of MB.

The formation of the HCR product was also investigated using gel electrophoresis analysis (Figure 2D). The lanes from left to right represent the PAGE results for sample 1, sample 2, sample 3, and the DNA marker. Small molecular weight DNA molecules were used for the probe DNA; therefore, one bright band appeared at the bottom of sample 1. Another bright band appeared at a higher position in sample 2, corresponding to the hybridization of probe DNA and output DNA, suggesting that output DNA had been obtained by walking amplification. Sample 3 exhibited an obvious band corresponding to the products of the HCR. Gel electrophoresis analysis demonstrated that upon incubation with the output DNAs, the dsDNA/G-quadruplexes structure was formed. The results showed consecutive bands with decreased mobility, consistent with different concentrations of HCR product. Thus, the PAGE results showed that the biosensor performed successfully to achieve DNA walker-amplification and HCR-amplification.

Under the optimized experimental conditions, the target miRNA (miR-486-5p) at different concentrations was added into the reaction system to evaluate the analytical performance of the biosensing platform. As illustrated in Figure 2E, the LSV peak current gradually increased with an increase in the miR-486-5p concentration, which was in accordance with the fact that higher concentrations of miRNA induce more HCR, and more MB is then bound within the G-quadruplex-incorporated duplex DNA chain to increase the peak current. Figure 2F shows there was a good linear correlation between the absolute value of the LSV peak current and the logarithm of the miR-486-5p concentration over the range from 20 fM to 5 nM. The correlation equation was determined to be $I = 0.567\mathrm{Lg}C_{miRNA} + 2.65$, with a correlation coefficient of $R^2 = 0.991$. Here, I is the LSV peak current (expressed in units of μA), and $\mathrm{Lg}C_{miRNA}$ is the logarithm of the miR-486-5p concentration (given in units of pM). The directly measured limit of detection for the miR-486-5p assay was 5.68 fM based on the 3σ per slope role.

To verify the specificity of the reaction system, a series of metal solutions were selected for control experiments. As shown in Figure 2G, in the presence of Mn^{2+}, the catalytic efficiency of the reaction was higher, and the electrochemical signal was stronger than in the absence of Mn^{2+}. The presence of other metal ions hardly resulted in any change to the peak value obtained by the detection system. These results indicated that, compared with other catalytic ions, Mn^{2+} was specific to the detection system and resulted in greater capture of electrochemical molecules. The selectivity of this assay was further investigated by the addition of mismatched sequences of miR-486-5p (mis-1, mis-2, and mis-3), miR-21, BSA, glucose, and peptide into the reaction system. As shown 2H, a high LSV peak current was detected in the presence of miR-486-5p. A significant drop in the LSV peak current was observed when interference was present. The results demonstrated that the miRNA biosensing approach showed high selectivity toward the target miRNA, even being able to distinguish between the target and a one-base mismatch. Thus, the proposed electrochemical miRNA assay exhibited high sequence specificity to discriminate target miRNA from similar miRNA molecules and other contaminants.

A comparison of different methods for miRNA detection is shown in Table S2 (Supporting Information), which indicated that our designed biosensor had a good performance. These results demonstrated that the sensitive detection of miRNA was realized by the developed electrochemical strategy, showing a wide linear range from 20 fM to 5 nM with a detection limit of 5.68 fM. Generally, miRNA detection is challenging because of the low abundance of miRNA in clinical samples (typically ≤ sub-nanomolar).[24] The dual signal amplification of the designed biosensor was capable of the detection limit and exhibited excellent selectivity even for single-base mismatched miRNA. Notably, it is possible to realize an easy test in a sample in-result out the manner by simplifying both the reagent components and the procedure steps.[25] For the simplification of reagent components, Au nanoparticles can be pre-functionalized with DNA strands (including DNAzyme, locking strand, and substrate strand) as a basic reagent, prior to the sample addition. In this way, once samples containing target miRNA are directly added, the released products will be filtered out after DNAzyme-cleavage signal amplification, and the output DNAs will hopefully be obtained. For the simplification of procedure steps, a printed electrochemical chip can be introduced and fabricated.[17b,26] In the current assay, the

© 2022 Wiley-VCH GmbH

16136829, 2022, 22, Downloaded from https://onlinelibrary.wiley.com/doi/10.1002/smll.202200784 by Egyptian National Sci. Network (Enstine), Wiley Online Library on [06/11/2022]. See the Terms and Conditions (https://onlinelibrary.wiley.com/terms-and-conditions) on Wiley Online Library for rules of use; OA articles are governed by the applicable Creative Commons License

electrochemical detection process was performed, including DNA probe modification, output DNAs hybridization, and MB signal combination. By pre-printing DNA probes onto an electrochemical chip through microarray technology, the electrochemical signals can be easily collected by directly adding the output DNAs and MB signal reagent onto the integrated chip and then sending the chip into an electrochemical workstation.

2.4. Profiling of MiRNA in NSCLC Cell Lines

We further used this method to profile the miR-486-5p expression levels in different types of NSCLC cell lines (H460, H1299, H1975, and H226 cells). The miR-486-5p concentrations in the NSCLC cell lines (**Figure 3**A) were detected based on the proposed method. A significant reduction in the expression of miR-486-5p was detected in the NSCLC cell lines, compared with normal cells (MRC5), consistent with previous reports that there is an inverse correlation between miR-486-5p expression and NSCLC progression.[27] We further used the standard RT-qPCR method to quantify the miR-486-5p concentrations in the NSCLC cell lines, and the obtained values were shown in Figure S4 (Supporting Information). As shown in Figure 3B, the miR-486-5p concentrations in the NSCLC cell lines was much less, decreased in the order of H460 > H1299 > H1975 > H226 cells. For the NSCLC cell lines, the obtained values of the proposed method were in agreement with those measured using the RT-qPCR method, affording a linear relationship with the Pearson correlation coefficients of 0.938 (Figure 3C). The discrepancy in the correlation could result in part from some level of miRNA loss or degradation during the extraction process, which also contributes to the greater variability of miRNA expression level detected.

In addition, we measured the miRNA in samples extracted from human lung adenocarcinoma cells which is the most common pathological type of NSCLC. A549 cells were selected as an example to validate the capability of the proposed assay for miRNA detection, which was commonly reported in previous literature.[28] Notably, in a logarithmic scale, the peak current difference exhibited a linear correlation with the number of cells in the range of 10–5000 cells (Figure 3D,E). To evaluate the accuracy of the method, we further investigated the applicability of the biosensor for miRNA detection in real serum samples. A known amount of miRNA (10 pM and 100 pM, respectively) was mixed with ten-fold diluted human serum samples, and the recoveries were detected using the developed method. The standard addition method was used to determine the recovery with an average value from 86.4% to 108.7% (Figure 3F), indicating that the developed approach can be used to achieve miRNA detection in an actual sample. These results clearly demonstrated that the biosensor was capable of being used to quantify miR-486-5p in real biological samples.

Circulating miRNAs are promising biomarkers for NSCLC diagnosis in a non-invasive manner. However, traditional RT-qPCR methods for miRNA analysis require expensive kits (about ≈$13 per sample) and complex procedures with limited

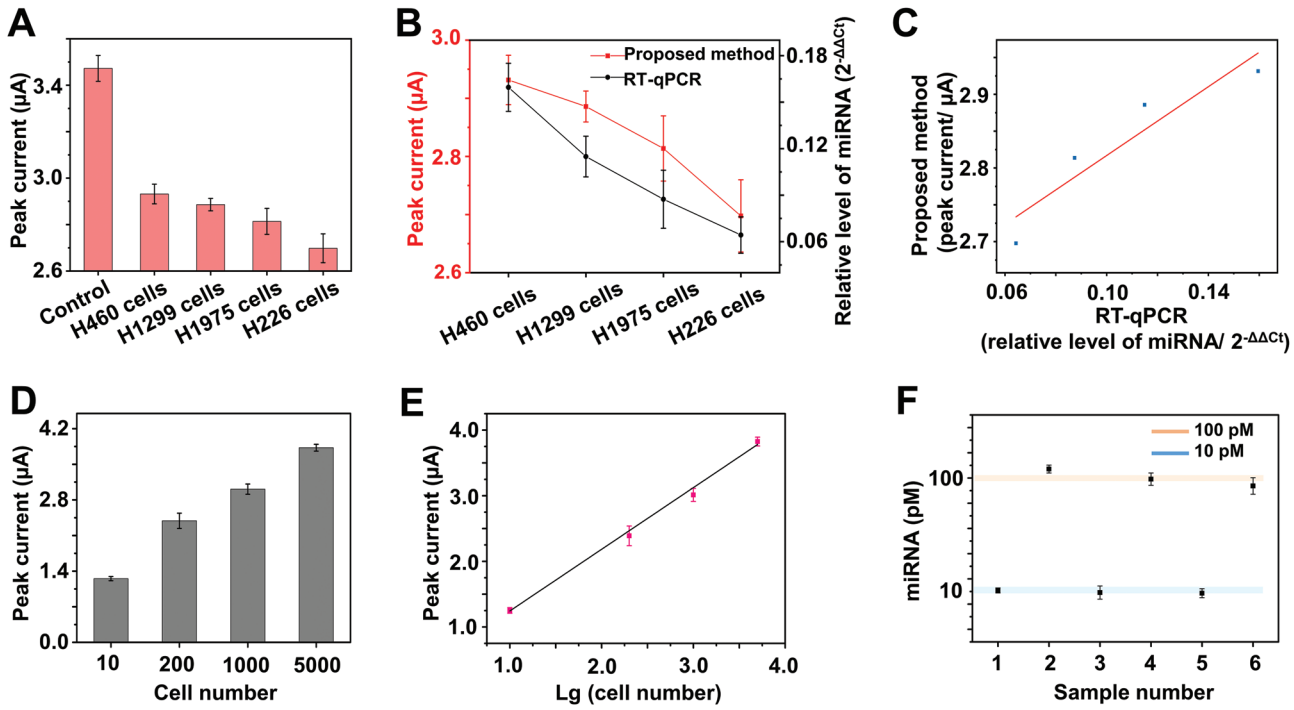

Figure 3. A) Measurement of miR-486-5p expression in different types of non-small cell lung cancer (NSCLC) cell lines (H460, H1299, H1975, and H226 cells) obtained by the proposed method. Normal cells (MRC5) were used as a control. B) Comparison of the proposed method and RT-qPCR method. C) Linear correlation between RT-qPCR method and the proposed method. *X* is the relative level of miRNA of the RT-qPCR method, *Y* is the linear sweep voltammetry (LSV) peak current (expressed in units of μA) of the proposed method. D) Measurement of miR-486-5p expression in different numbers of A549 cells (from 10 to 5000). E) Linear correlation between the peak current and the logarithm of the number of A549 cells. F) Serum measurement of miR-486-5p expression using the standard addition method. Error bars are the standard derivation obtained from three independent experiments.

© 2022 Wiley-VCH GmbH

16136829, 2022, 22, Downloaded from https://onlinelibrary.wiley.com/doi/10.1002/smll.202200784 by Egyptian National Sci. Network (Enstine), Wiley Online Library on [06/11/2022]. See the Terms and Conditions (https://onlinelibrary.wiley.com/terms-and-conditions) on Wiley Online Library for rules of use; OA articles are governed by the applicable Creative Commons License

sensitivity (relative quantitative values by $2^{-\Delta\Delta Ct}$), which are difficult to access in clinics.[29] In contrast, the versatile electrochemical biosensing system displayed many advantages, such as a simple fabrication process (two steps on the electrode), easy preparation (commonly used nanomaterials of AuNPs), and low cost (≈$1 per sample). As a result, the method would have the potential for clinical application.

2.5. Early Diagnosis and Prognosis for NSCLC

The differential expression of miR-486-5p in human serum is recognized as a potential predictor for NSCLC as the miR-486-5p expression level is frequently reduced in NSCLC. To further investigate the clinical use of the proposed platform, we studied a NSCLC patient cohort ($n = 75$; 15 healthy controls and 60 patients with stage I–IV NSCLC) and analyzed three types of NSCLC, including large cell lung cancer (LCLC, $n = 20$), lung adenocarcinoma (LA, $n = 20$), and squamous cell carcinoma of lung cancer (SQCLC, $n = 20$). Circulating miRNAs were initially released and subsequently measured in the serum lysate supernatants, and the miR-486-5p concentrations were detected based on the electrochemical method. The heat map in **Figure 4**A summarizes the normalized signals of four stages of NSCLC, in which the expression level of the miRNA is indicated by the color intensity. As shown in Figure 4B, each stage of LC showed a heterogeneous reduction in the level of miR-486-5p markers, in contrast with the high expression in healthy controls (*t*-test, $p < 0.001$). These results demonstrated that miR-486-5p is a potential marker for predicting NSCLC and were consistent with previous research that miR-486-5p functions as a tumor suppressor that can inhibit the occurrence and metastasis of LC. The diagnostic efficacy was also analyzed using a ROC curve. As shown in Figure 4C, the AUC of miR-486-5p was 0.879 (95%CI: 0.749-1.000), with a sensitivity of 80.0% and a specificity of 78.6% for discrimination of early NSCLC patients from healthy controls. The combination (SUM) of miR-486-5p and six clinically-acceptable protein tumor markers (CEA, CA125, SCC, NSE, Pro-GRP, and CYFRA21-1) showed higher accuracy (AUC: 1.000) than a single miRNA marker or six tumor markers for identifying patients with NSCLC. In conclusion, the developed platform provides a viable alternative to current methods for determining the clinical diagnosis and prognosis of NSCLC. We further performed the blind test to further validate the miRNA marker, which is a key step for its clinical translation and clinical trial. In detail, we recruited an independent cohort for the external validation of the proposed platform. Notably, all the samples from the cohort were blindly coded with a random mixture of cancer group ($n = 16$) and healthy controls ($n = 4$). As a result, the platform yielded a consistent diagnostic performance with the previous results, with an overall accuracy of 85.0% for the blind test (Figure S5, Supporting Information). We performed power analysis to validate enough serum sample size of the clinical patients in this work. When the total number of samples reached 30, the predicted power achieved ≈0.863 (Figure S6, Supporting Information). The calculation results indicated that the sample size could be used for effective analysis and validation of our proposed platform.

As shown in Figure 4D, we also studied patient cohorts that had NSCLC diagnosis: benign disease ($n = 15$); cancer without treatment ($n = 15$); and cancer with treatment (recurrence: $n = 15$; no recurrence: $n = 15$). As shown in Figure 4E, NSCLC patients had decreased levels of miR-486-5p compared with patients with benign disease ($p < 0.0001$). In discriminating between early NSCLC (stage I, no treatment) and benign disease, the single miRNA marker was superior to six serum tumor markers, with the sensitivity of 86.7% and specificity of 73.3%. The AUC of the miR-486-5p was 0.907 (95%CI: 0.805-1.000), while the combined multiple biomarkers had an AUC of 1.000 (Figure 4F). Of particular interest was that the combination of these biomarkers (SUM) was superior to both types of markers individually. These results suggested that the miR-486-5p level could provide critical information to avoid the need for NSCLC biopsies. Next, we explored the capability of miR-486-5p to biochemically detect the recurrence of cancer after the radical operation. We summarized the performance of miR-486-5p profiles in differentiating between NSCLC with recurrence and no recurrence. The value of the combined multiple biomarkers was significantly higher in the recurrence group compared with the no recurrence group ($p < 0.0001$; Figure 4E). Therefore, miR-486-5p could also act.

In a clinical cohort ($n = 75$), the sensitivity, specificity, and accuracy in detecting stage I cancers by the proposed method are 80.0%, 78.6%, and 87.9%, respectively. In parallel, the platform was able to distinguish NSCLC patients (stage I, no treatment) from those with benign disease with a sensitivity of 86.7%, specificity of 73.3%, and accuracy of 90.7%. We also demonstrated the possibility of NSCLC diagnosis by the combination of miRNA and six protein markers, and the higher accuracies (AUC: 1.000) were obtained. Early detection of NSCLC can improve the survival rate and reduce the costs of management of the disease.[30] However, conventional diagnostics using protein biomarkers are limited considering the detection sensitivity, diagnosis accuracy, and operation process, particularly for early-stage of LC. As the proposed method can provide important information for early-stage cancer detection and monitoring of cancer recurrence via assaying miRNA, it would be feasible to implement the proposed method in a routine diagnostic setting.

3. Conclusion

We have developed a versatile electrochemical biosensing strategy for the sensitive detection of miRNA based on Mn^{2+}-powered DNAzyme and DNA-walker-induced HCR multiple signal amplification. This method converted GSH to a metal-ion target for determination, combined with cycling amplification driven by a DNA walker. In addition, this method introduced a G-quadruplex structure to the HCR signal amplification, which induced larger changes in the electrochemical signal and improved the sensitivity of the method. This biosensing strategy exhibited excellent selectivity and could distinguish between the target and single-base mismatched miRNA. By profiling miRNA in the NSCLC cohort, this designed strategy showed high efficiency not only for lung tumor early diagnosis but also for the discrimination of NSCLC and benign

© 2022 Wiley-VCH GmbH

16136829, 2022, 22, Downloaded from https://onlinelibrary.wiley.com/doi/10.1002/smll.202200784 by Egyptian National Sci. Network (Enstine), Wiley Online Library on [06/11/2022]. See the Terms and Conditions (https://onlinelibrary.wiley.com/terms-and-conditions) on Wiley Online Library for rules of use; OA articles are governed by the applicable Creative Commons License

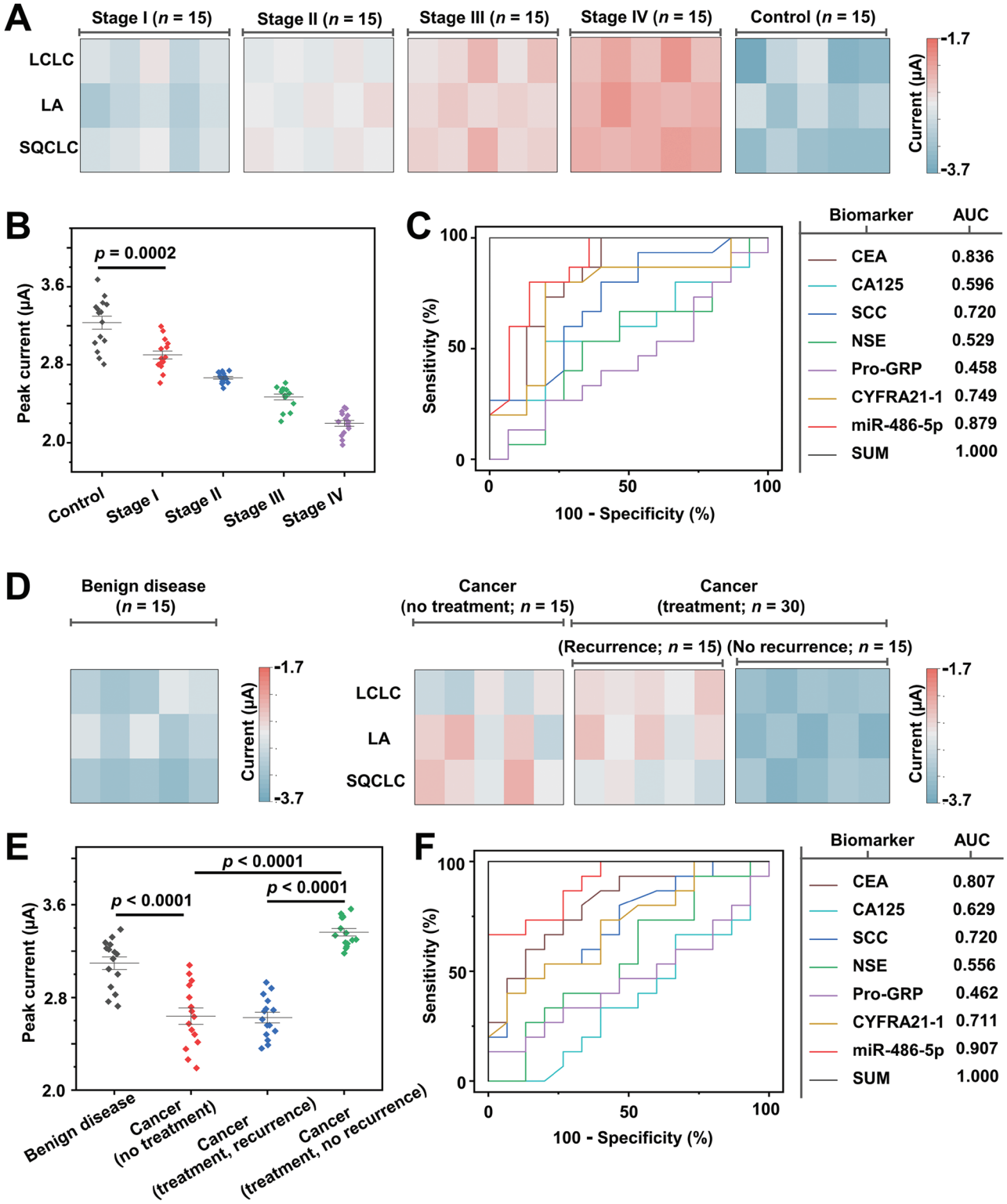

Figure 4. A) Profiling of miR-486-5p concentrations for lung tumor classification, heat map of miRNA profiling in healthy controls ($n = 15$) and patients with non-small cell lung cancer (NSCLC) at stage I ($n = 15$), stage II ($n = 15$), stage III ($n = 15$), and stage IV ($n = 15$). B) LSV signal for miRNAs in different stages of the lung tumor cohort (mean ± SD). C) ROC curve of miRNA marker, six tumor markers, and combined multiple biomarkers (SUM) for early diagnosis of NSCLC (stage I) from a healthy donor. D) Results of miR-486-5p detection in a lung tumor cohort, heat map of miRNA detection in patients with benign disease ($n = 15$), patients with NSCLC without treatment ($n = 15$), patients with treatment and recurrence ($n = 15$), and patients with treatment and no recurrence ($n = 15$). E) LSV signal for miRNAs in the lung tumor cohort (mean ± SD). F) ROC curve of the miRNA marker, six tumor markers, and combined multiple biomarkers (SUM) for discrimination of NSCLC (stage I, no treatment) and benign disease. The statistical differences in B and E were determined by a two-tailed Student's *t*-test. The *p* values are indicated in the charts.

© 2022 Wiley-VCH GmbH

16136829, 2022, 22, Downloaded from https://onlinelibrary.wiley.com/doi/10.1002/smll.202200784 by Egyptian National Sci. Network (Enstine), Wiley Online Library on [06/11/2022]. See the Terms and Conditions (https://onlinelibrary.wiley.com/terms-and-conditions) on Wiley Online Library for rules of use; OA articles are governed by the applicable Creative Commons License

disease, which was superior to the analysis of other six tumor markers. Therefore, the developed platform has more promise for application in NSCLC diagnosis and prognosis.

4. Experimental Section

Electrode Preparation and Electrochemical Measurements: A gold electrode (2 mm) was pretreated with piranha solution (98% H_2SO_4: 30% H_2O_2 = 3: 1) for 5 min (caution: the piranha solution reacts violently). Next, the electrode was polished to a mirror-like surface with P4000 silicon carbide paper and then 1, 0.3, and 0.05 mm alumina slurry sequentially. The electrode was sonicated in ethanol and ultrapure water for 5 min each. Subsequently, the electrode was electrochemically cleaned with 0.5 M H_2SO_4 for 20 cycles to remove any remaining impurities. Then, the electrode was dried with nitrogen to give a working electrode surface that was ready to use. All electrochemical measurements were carried out with a CS 300X workstation (Corrtest Instruments, China). The conventional three-electrode system consisted of a DNA-bound gold working electrode, an Ag/AgCl reference electrode, and a platinum auxiliary electrode. Linear sweep voltammetry (LSV) was performed in 20 mM Tris-HCl (140 mM NaCl, 5 mM $MgCl_2$, pH 7.4). Electrochemical impedance spectroscopy (EIS) and cyclic voltammetry (CV) measurements were performed in 5 mM $[Fe(CN)_6]^{3-/4-}$ and 1 M KCl buffer. The experimental parameters were as follows. LSV: scan rate 50 mV s^{-1}; EIS: bias potential 0.232 V, amplitude 5 mV, frequency range 0.1–100000 Hz; and CV: sweep range 0.6 to –0.2 V, scan rate 50 mV s^{-1}.

DNAzyme-Cleavage Cycling Amplification Reaction: GSH was used to reduce MnO_2 nanosheets to Mn^{2+}. GSH (10 μM) and MnO_2 nanosheet solutions were mixed for 3 min, and then the mixture was centrifuged at 10000 rpm for 5 min. The obtained supernatant with Mn^{2+} was used as the GSH sample solution. Then, the DNAzyme-cleavage cycling amplification reaction was performed. Here, 50 μL of gold nanoparticles (AuNPs) were centrifuged at 10000 rpm for 15 min and resuspended in 100 μL of ultrapure water. To make the DNA walker inactive, 1 μM DNAzyme strand (*D*) and 1 μM locking strand (*L*) were incubated at 37 °C for 1 h to form the D/L duplex. Then, a mixture of substrate strand (S, 1 μM) and D/L duplex (1 μM) at a 20:1 volume ratio was incubated with AuNPs at 37 °C for 12 h to form a DNA walker structure. Subsequently, the mixture was centrifuged (10000 rpm, 10 min) to remove the uncoupled single-stranded DNA, and the remaining AuNP-S-D/L DNA conjugates were dispersed in 150 μL of buffer solution. Next, different concentrations of miRNA (miR-486-5p) were added to the solution for 1 h, forming a miRNA/locking strand duplex which was released into the solution. After centrifugation, 5 μL of the above GSH sample solution was mixed with 20 μL of the AuNP-S-D solution and incubated at 37 °C for 90 min. The product was separated by centrifugation at 10000 rpm for 10 min, and the supernatants containing different concentrations of output DNA were collected and used as the miRNA sample solutions.

HCR-Amplified Electrochemical MicroRNA (miRNA) Assay: The electrode was modified with 1 μM probe DNA at room temperature overnight, followed by blocking with 1 mM mercaptoethanol (MCH) for 30 min. Then, 20 μL of the miRNA sample solution, as described above, at various concentrations was dropped onto the modified electrode at 37 °C for 1 h and washed with Tris-HCl (pH 7.4). Next, 150 μL of a mixture containing 2 μM H1 (Hairpin DNA1), 2 μM H2 (Hairpin DNA2), 25 mM KCl, and 50 μM MB was dropped onto the obtained electrode. The reaction solution was incubated at 37 °C for 2 h before the electrochemical measurements. A control experiment was prepared separately and performed under the same conditions. All experiments were repeated three times.

Polyacrylamide gel electrophoresis analysis (PAGE) was performed to characterize the DNA walker-induced HCR amplification process. First, the miRNA sample solution was obtained by subjecting 200 nM miRNA to a DNAzyme-cleavage cycling reaction. Then, 10 μL of sample 1 (10 μM probe DNA), 10 μL of sample 2 (10 μM probe DNA and miRNA sample solution), and 10 μL of sample 3 (10 μM probe DNA, miRNA sample solution, 20 μM H1, and 20 μM H2) were placed on a 12% polyacrylamide gel. The electrophoresis was performed in 0.5 × TBE (pH 8.0) at 100 V constant voltage for 1.5 h. After EB staining, the gel was scanned using a gel imaging analyzer.

Detection of miRNA in Human Clinical Samples: Lung cancer (LC) cell lines (A549, H460, H1299, H1975, and H226 cells) and normal cells (MRC5) were cultured in Dulbecco's modified Eagle's medium (Gibco, USA) supplemented with 10% fetal bovine serum (Gibco) in 5% CO_2 in an incubator at 37 °C. At the exponential growth phase, cells were collected with trypsinization and centrifuged at 1000 rpm for 5 min. The miRNAs were extracted from the cancer cells using a miRNeasy Mini Kit (Qiagen, Hilden, Germany). For clinical applications, the miRNAs from the serum of healthy persons, benign diseases, and non-small cell LC (NSCLC) patients were extracted using a miRNeasy Serum/Plasma Kit (Qiagen) for isolation. In particular, benign diseases included pneumonia (n = 5), bronchitis (n = 4), pulmonary abscess (n = 1), and pulmonary nodule (n = 5). Finally, the RNA extracts were stored at –80 °C or mixed with a reaction solution for measurement. To check the practical utility of the method, diluted human serum samples spiked with miRNA were used instead of the standard miRNA solutions. Before the signal amplification reaction, a ten-fold diluted serum sample was mixed with 10 μL of miRNA at different concentrations. The electrochemical signal was detected using the prepared biosensor. Human serum samples were collected at the Shanghai Chest Hospital. All relevant ethical regulations were complied with. The study was approved by the Ethics Committee at the Shanghai Chest Hospital. Written informed consent was obtained for all participants. All samples were anonymized, and relevant pathological diagnoses were recorded (Table S3 and S4, Supporting Information).

Statistical Analysis: All statistical analysis in this work (including significance analyses, ROC curve construction, and AUC calculation) was performed on IBM SPSS Statistics software (Version 26.0.0). Sensitivity stood for the probability that when cancer was detected with a positive result (true positive rate), specificity as the probability that when cancer was not detected with a negative result (true negative rate), and accuracy as the overall probability that one sample was correctly classified. The 95% CIs were calculated using a binomial distribution. The significance of the difference (p-value) between the test profiles was calculated using a two-tailed Student's t-test. All mean values reported were obtained from the average of the data set, and the errors represent one standard deviation (SD). Plots and charts were performed using Origin 2021 software. A power analysis (a universal method to derive the optimal sample size by estimating statistical power in a hypothesis test) on a dataset from a pilot study of 30 samples (15 /15, NSCLC/control) to compute the minimum sample number required for a meaningful diagnosis was also included.

Supporting Information

Supporting Information is available from the Wiley Online Library or from the author.

Acknowledgements

F.M., W.Y., and C.C. contributed equally to this work. The authors are grateful for the financial support from Projects 2021YFA0910100, 2021YFF0703500, 2017YFE0124400, and 2017YFC0909000 by the National Key R&D Program of China, and Project 2021-01-07-00-02-E00083 by Shanghai Institutions of Higher Learning. This work was also sponsored by the Shanghai Rising-Star Programme (19QA1404800), Innovation Group Project of Shanghai Municipal Health Commission (2019CXJQ03 and 20194Y0317), Innovation Research Plan by the Shanghai Municipal Education Commission (ZXWF082101), the Science and Technology Commission of Shanghai Municipality (21YF1443000), National Research Center for Translational Medicine Shanghai (TMSK-2021-124 and

© 2022 Wiley-VCH GmbH

16136829, 2022, 22, Downloaded from https://onlinelibrary.wiley.com/doi/10.1002/smll.202200784 by Egyptian National Sci. Network (Enstine), Wiley Online Library on [06/11/2022]. See the Terms and Conditions (https://onlinelibrary.wiley.com/terms-and-conditions) on Wiley Online Library for rules of use; OA articles are governed by the applicable Creative Commons License

NRCTM(SH)-2021-06), and Medical-Engineering Joint Funds of Shanghai Jiao Tong University (YG2019QNA44, YG2021ZD09, and YG2022QN107).

Conflict of Interest

The authors declare no conflict of interest.

Data Availability Statement

The data that support the findings of this study are available from the corresponding author upon reasonable request.

Keywords

DNAzymes, early diagnosis, hybridization chain reaction, lung cancer, microRNAs

Received: February 6, 2022
Revised: March 1, 2022
Published online: March 25, 2022

[1] F. Bray, J. Ferlay, I. Soerjomataram, R. L. Siegel, L. A. Torre, A. Jemal, *Ca-Cancer J. Clin.* **2018**, *68*, 394.
[2] R. L. Siegel, K. D. Miller, A. Jemal, *CaCancer J. Clin.* **2019**, *69*, 7.
[3] C. Wang, S. Tan, J. Li, W. R. Liu, Y. Peng, W. Li, *Cancer Lett.* **2020**, *492*, 106.
[4] a) C. Alix-Panabières, K. Pantel, *Cancer Discovery* **2016**, *6*, 479; b) G. Siravegna, S. Marsoni, S. Siena, A. Bardelli, *Nat. Rev. Clin. Oncol.* **2017**, *14*, 531; c) S. Jiang, K. Huang, J. Qu, J. Lin, P. Huang, *View* **2020**, *2*, 20200075.
[5] a) D. Ardila, A. P. Kiraly, S. Bharadwaj, B. Choi, J. J. Reicher, L. Peng, D. Tse, M. Etemadi, W. Ye, G. Corrado, D. P. Naidich, S. Shetty, *Nat. Med.* **2019**, *25*, 954; b) M. Reck, K. F. Rabe, *N. Engl. J. Med.* **2017**, *377*, 849; c) J. Cao, X. Shi, D. D. Gurav, L. Huang, H. Su, K. Li, J. Niu, M. Zhang, Q. Wang, M. J. Jiang, K. Qian, *Adv. Mater.* **2020**, *32*, 2000906.
[6] a) S. Sun, W. Liu, J. Yang, H. Wang, K. Qian, *Angew. Chem.* **2021**, *60*, 11310; b) L. Huang, K. Qian, *Small Methods* **2020**, *4*, 1900717.
[7] a) E. Heitzer, I. S. Haque, C. E. Roberts, M. R. Speicher, *Nat. Rev. Genet.* **2019**, *20*, 71; b) L. M. Seijo, N. Peled, D. Ajona, M. Boeri, J. K. Field, G. Sozzi, R. Pio, J. J. Zulueta, A. Spira, P. P. Massion, P. J. Mazzone, L. M. Montuenga, *J. Thorac. Oncol.* **2019**, *14*, 343; c) W. Li, J. B. Liu, L. K. Hou, F. Yu, J. Zhang, W. Wu, X. M. Tang, F. Sun, H. M. Lu, J. Deng, J. Bai, J. Li, C. Y. Wu, Q. L. Lin, Z. W. Lv, G. R. Wang, G. X. Jiang, Y. S. Ma, D. Fu, *Mol. Cancer* **2022**, *21*, 25.
[8] a) G. Yang, Z. Xiao, C. Tang, Y. Deng, H. Huang, Z. He, *Biosens. Bioelectron.* **2019**, *141*, 111416; b) L. Rong, Q. Lei, X. Z. Zhang, *View* **2020**, *1*, 20200050.
[9] a) D. P. Bartel, *Cell* **2009**, *136*, 215; b) L. He, J. M. Thomson, M. T. Hemann, E. Hernando-Monge, D. Mu, S. Goodson, S. Powers, C. Cordon-Cardo, S. W. Lowe, G. J. Hannon, S. M. Hammond, *Nature* **2005**, *435*, 828.
[10] a) Z. Shabaninejad, F. Yousefi, A. Movahedpour, Y. Ghasemi, S. Dokanehiifard, S. Rezaei, R. Aryan, A. Savardashtaki, H. Mirzaei, *Anal. Biochem.* **2019**, *581*, 113349; b) S. Kim, J.-E. Park, W. Hwang, J. Seo, Y.-K. Lee, J.-H. Hwang, J.-M. Nam, *J. Am. Chem. Soc.* **2017**, *139*, 3558; c) T. Jet, G. Gines, Y. Rondelez, V. Taly, *Chem. Soc. Rev.* **2021**, *50*, 4141.
[11] a) A. D. Castañeda, N. J. Brenes, A. Kondajji, R. M. Crooks, *J. Am. Chem. Soc.* **2017**, *139*, 7657; b) X. Xie, Z. Wang, M. Zhou, Y. Xing, Y. Chen, J. Huang, K. Cai, J. Zhang, *Small Methods* **2021**, *5*, 2101072; c) S. Kogikoski, W. J. Paschoalino, L. Cantelli, W. Silva, L. T. Kubota, *TrAC, Trends Anal. Chem.* **2019**, *118*, 597; d) X. Liu, J. Liu, *View* **2020**, *2*, 20200102.
[12] W. Xu, J. Lin, M. Gao, Y. Chen, J. Cao, J. Pu, L. Huang, J. Zhao, K. Qian, *Adv. Sci.* **2020**, *7*, 2002021.
[13] a) Y. Zhang, W. Wang, Z. Lin, B. Liu, X. Zhou, *Biosens. Bioelectron.* **2020**, *161*, 112256; b) V. Vedarethinam, L. Huang, M. Zhang, H. Su, H. Hu, H. Xia, Y. Liu, B. Wu, X. Wan, J. Shen, L. Xu, W. Liu, J. Ma, K. Qian, *Adv. Funct. Mater.* **2020**, *30*, 2002791; c) F. Yin, F. Wang, C. Fan, X. Zuo, Q. Li, *View* **2020**, *2*, 20200038.
[14] a) Q. Wang, Y. Liu, X. Wang, F. Wang, L. Zhang, S. Ge, J. Yu, *ACS Appl. Mater. Interfaces* **2021**, *13*, 25783; b) X. Qu, D. Zhu, G. Yao, S. Su, J. Chao, H. Liu, X. Zuo, L. Wang, J. Shi, L. Wang, W. Huang, H. Pei, C. Fan, *Angew. Chem.* **2017**, *56*, 1855; c) R. Yang, G. Jiang, H. Liu, L. He, F. Yu, L. Liu, L. Qu, Y. Wu, *Biosens. Bioelectron.* **2021**, *188*, 113337.
[15] a) C. A. Figg, P. H. Winegar, O. G. Hayes, C. A. Mirkin, *J. Am. Chem. Soc.* **2020**, *142*, 8596; b) J. R. Wang, C. Xia, L. Yang, Y. F. Li, C. M. Li, C. Z. Huang, *Anal. Chem.* **2020**, *92*, 4046.
[16] a) K. K. Reddy, H. Bandal, M. Satyanarayana, K. Y. Goud, K. V. Gobi, T. Jayaramudu, J. Amalraj, H. Kim, *Adv. Sci.* **2020**, *7*, 1902980; b) S. Liu, C. Lai, X. Liu, B. Li, C. Zhang, L. Qin, D. Huang, H. Yi, M. Zhang, L. Li, W. Wang, X. Zhou, L. Chen, *Coord. Chem. Rev.* **2020**, *424*, 213520; c) Y. Kim, H. Choi, J. E. Shin, G. Bae, R. Thangam, H. Kang, *View* **2020**, *1*, 20200029.
[17] a) Y. Wang, B. Li, T. Tian, Y. Liu, J. Zhang, K. Qian, *TrAC, Trends Anal. Chem.* **2022**, *149*, 116565; b) W. Shu, Y. Wang, C. Liu, R. Li, C. Pei, W. Lou, S. Lin, W. Di, J. Wan, *Small Methods* **2020**, *4*, 1900469.
[18] a) C. Zhu, D. Liu, Y. Li, X. Shen, S. Ma, Y. Liu, T. You, *Biosens. Bioelectron.* **2020**, *150*, 111814; b) M. Li, C. Xiong, Y. Zheng, W. Liang, R. Yuan, Y. Chai, *Anal. Chem.* **2018**, *90*, 8211; c) F.-T. Zhang, J. Nie, D.-W. Zhang, J.-T. Chen, Y.-L. Zhou, X.-X. Zhang, *Anal. Chem.* **2014**, *86*, 9489; d) L. Miccio, F. Cimmino, I. Kurelac, M. M. Villone, V. Bianco, P. Memmolo, F. Merola, M. Mugnano, M. Capasso, A. Iolascon, P. L. Maffettone, P. Ferraro, *View* **2020**, *1*, 20200034.
[19] F. Meng, Y. Xu, W. Dong, Y. Tang, P. Miao, *Mikrochim. Acta* **2018**, *185*, 398.
[20] J. Fang, C. Yuan, J. Li, J. Li, T. Yang, Y. Guo, D. Wang, J. Xue, W. Fu, G. Xie, *Biosens. Bioelectron.* **2021**, *177*, 112981.
[21] J. Chen, Z. Luo, C. Sun, Z. Huang, C. Zhou, S. Yin, Y. Duan, Y. Li, *TrAC, Trends Anal. Chem.* **2019**, *120*, 115626.
[22] a) M. Zhang, L. Huang, J. Yang, W. Xu, H. Su, J. Cao, Q. Wang, J. Pu, K. Qian, *Adv. Sci.* **2021**, *8*, 2101333; b) C. Pei, C. Liu, Y. Wang, D. Cheng, R. Li, W. Shu, C. Zhang, W. Hu, A. Jin, Y. Yang, J. Wan, *Angew. Chem.* **2020**, *132*, 10923; c) R. Li, Y. Zhou, C. Liu, C. Pei, W. Shu, C. Zhang, L. Liu, L. Zhou, J. Wan, *Angew. Chem.* **2021**, *133*, 12612.
[23] M. Y. Lucero, J. Chan, *Nat. Chem.* **2021**, *13*, 1248.
[24] a) R. Bruch, J. Baaske, C. Chatelle, M. Meirich, S. Madlener, W. Weber, C. Dincer, G. A. Urban, *Adv. Mater.* **2019**, *31*, 1905311; b) S. Cai, T. Pataillot-Meakin, A. Shibakawa, R. Ren, C. L. Bevan, S. Ladame, A. P. Ivanov, J. B. Edel, *Nat. Commun.* **2021**, *12*, 3515.
[25] a) L. Huang, D. D. Gurav, S. Wu, W. Xu, V. Vedarethinam, J. Yang, H. Su, X. Wan, Y. Fang, B. Shen, C.-A. H. Price, E. Velliou, J. Liu, K. Qian, *Matter* **2019**, *1*, 1669; b) L. M. Teixeira, L. Mezzanotte, *View* **2021**, *2*, 20200177.
[26] W. Xu, L. Wang, R. Zhang, X. Sun, L. Huang, H. Su, X. Wei, C.-C. Chen, J. Lou, H. Dai, Kun, Qian , *Nat. Commun.* **2020**, *11*, 1.

 © 2022 Wiley-VCH GmbH

16136829, 2022, 22, Downloaded from https://onlinelibrary.wiley.com/doi/10.1002/smll.202200784 by Egyptian National Sci. Network (Enstine), Wiley Online Library on [06/11/2022]. See the Terms and Conditions (https://onlinelibrary.wiley.com/terms-and-conditions) on Wiley Online Library for rules of use; OA articles are governed by the applicable Creative Commons License

[27] a) L. J. Wang, M. Ren, H. X. Wang, J. G. Qiu, B. Jiang, C. Y. Zhang, *Anal. Chem.* **2020**, *92*, 8546; b) J. Wang, X. Tian, R. Han, X. Zhang, X. Wang, H. Shen, L. Xue, Y. Liu, X. Yan, J. Shen, *Oncogene* **2014**, *33*, 1181; c) X. Jin, W. Pang, Q. Zhang, H. Huang, *J. Int. Med. Res.* **2019**, *47*, 3745.

[28] P. Sidambaram, J. Colleran, *Biosens. Bioelectron.* **2020**, 112876.

[29] L. Ying, L. Du, R. Zou, L. Shi, N. Zhang, J. Jin, C. Xu, F. Zhang, C. Zhu, J. Wu, *Proc. Natl. Acad. Sci. USA* **2020**, *117*, 25036.

[30] L. Huang, L. Wang, X. Hu, S. Chen, Y. Tao, H. Su, J. Yang, W. Xu, V. Vedarethinam, S. Wu, B. Liu, X. Wan, J. Lou, Q. Wang, K. Qian, *Nat. Commun.* **2020**, *11*, 3556.

© 2022 Wiley-VCH GmbH

16136829, 2022, 22, Downloaded from https://onlinelibrary.wiley.com/doi/10.1002/smll.202200784 by Egyptian National Sci. Network (Enstine), Wiley Online Library on [06/11/2022]. See the Terms and Conditions (https://onlinelibrary.wiley.com/terms-and-conditions) on Wiley Online Library for rules of use; OA articles are governed by the applicable Creative Commons License